

# A 5-GHz CMOS Wireless LAN Receiver Front End

Hirad Samavati, *Student Member, IEEE*, Hamid R. Rategh, *Student Member, IEEE*, and Thomas H. Lee, *Member, IEEE*

**Abstract**—This paper presents a 12.4-mW front end for a 5-GHz wireless LAN receiver fabricated in a 0.24- $\mu\text{m}$  CMOS technology. It consists of a low-noise amplifier (LNA), mixers, and an automatically tuned third-order filter controlled by a low-power phase-locked loop. The filter attenuates the image signal by an additional 12 dB beyond what can be achieved by an image-reject architecture. The filter also reduces the noise contribution of the cascode devices in the LNA core. The LNA/filter combination has a noise figure of 4.8 dB, and the overall noise figure of the signal path is 5.2 dB. The overall IIP3 is  $-2$  dBm.

**Index Terms**—Automatic tuning, CMOS analog integrated circuits, high-frequency filters, HIPERLAN, image-reject circuits, low-noise amplifier (LNA), notch filter, receiver front end.

## I. INTRODUCTION

THE GROWING popularity of notebook computers demands high data-rate wireless LAN systems. Many existing wireless LAN systems operate in the 2.4-GHz ISM band. These products currently achieve maximum data rates of 1–2 Mbits/s. The need for higher data-rate wireless LAN products prompted the Federal Communications Commission (FCC) to release 300 MHz of spectrum for the unlicensed national information infrastructure (U-NII)[1]. Using this newly released frequency band, wireless LAN systems can provide data rates of several tens of megabits per second. The allocated frequencies overlap the European standard for the high-performance radio LAN (HIPERLAN) frequency band as shown in Fig. 1(a).

The superheterodyne architecture is the most widely used architecture for wireless receivers. Monolithic image cancellation has always been a challenge due to the design problems of on-chip filters. The use of image-reject architectures alleviates this problem to some extent. Typically, these architectures can practically achieve 30–40 dB of image cancellation [2], [3].

This paper describes the design and implementation of a 12.4-mW CMOS front-end receiver for a 5-GHz wireless LAN system. The receiver uses a tunable third-order filter, which is automatically tuned by an image-reject phase-locked loop (PLL), to alter the transfer function of the low-noise amplifier (LNA). The LNA/filter combination provides an additional 12 dB of image rejection beyond what can be achieved by an image-reject architecture.

## II. RECEIVER ARCHITECTURE

Wireless LAN systems require receiver architectures with wide dynamic range. When a transmitter and receiver are close

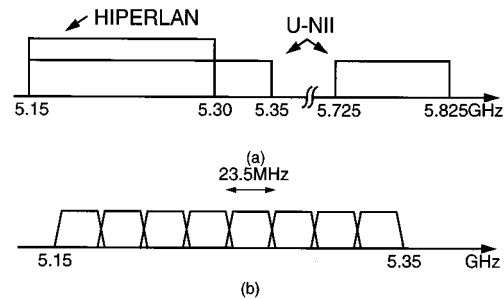


Fig. 1. (a) U-NII and HIPERLAN frequency bands (b) proposed channel allocation.

to each other, the received signal strength can be as high as  $-20$  dBm. A highly linear receiver is needed to accommodate such strong signals. On the other hand, the received signal can be quite weak due to fading. The receiver must be sensitive enough to detect signals as small as  $-148$  dBm/Hz. (i.e.,  $-74$  dBm for a 24-MHz bandwidth signal [7]). To have a predetection signal-to-noise ratio (SNR) of at least 12 dB, the overall noise figure of the receiver must be better than

$$NF = -148 \text{ dBm/Hz} - 12 \text{ dB} - (-174 \text{ dBm/Hz}) = 14 \text{ dB}$$

where  $-174$  dBm/Hz is the available noise power of the source. This noise figure is readily achievable in CMOS with a reasonably low power consumption.

The receiver uses the channel allocation depicted in Fig. 1(b) where the lower 200 MHz of the U-NII band is divided into eight channels, each 23.5 MHz wide. This choice of channel spacing is fully compatible with the HIPERLAN standard.

Fig. 2 shows the block diagram of the receive path. The system uses two sets of local oscillators (LO's) to implement an image reject architecture commonly known as the Weaver architecture. The LNA is followed by a first set of mixers to produce the  $I$  and  $Q$  components of the intermediate-frequency (IF) signal. A tunable third-order filter alters the transfer characteristic of the LNA to achieve further attenuation of the image signal. A PLL automatically tunes the image-reject band of the filter to the image frequency [4]–[6].

It is important to mention that the circuit implementations of the voltage-controlled oscillator (VCO) and the filter are exactly the same. Because of this similarity, the locations of the pole and zero of the filter are closely related to the oscillation frequency of the VCO. The VCO and the filter share the same control voltage, and since they are topologically identical, locking the VCO frequency to the frequency of the image signal tunes the notch frequency of the filter to the image frequency.

A passive mixer downconverts the VCO output by mixing it with the first LO. A phase/frequency detector (PFD) compares the downconverted signal against the second LO. A charge-pump circuit and loop filter complete the PLL. The lock

Manuscript received August 9, 1999; revised November 24, 1999. This work was supported by IBM Corporation and Stanford Graduate Fellowship Program.

The authors are with the Center for Integrated Systems, Stanford University, Stanford, CA 94305-4070 USA.

Publisher Item Identifier S 0018-9200(00)02991-7.



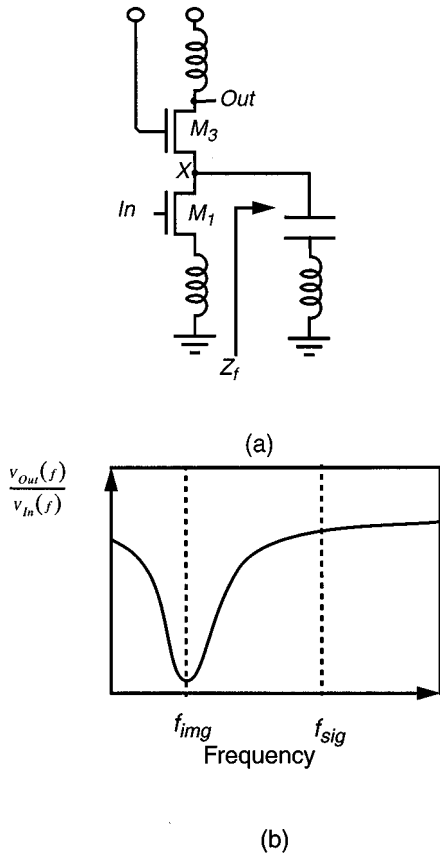


Fig. 4. (a) Image-reject LNA and (b) transfer function of the image-reject LNA.

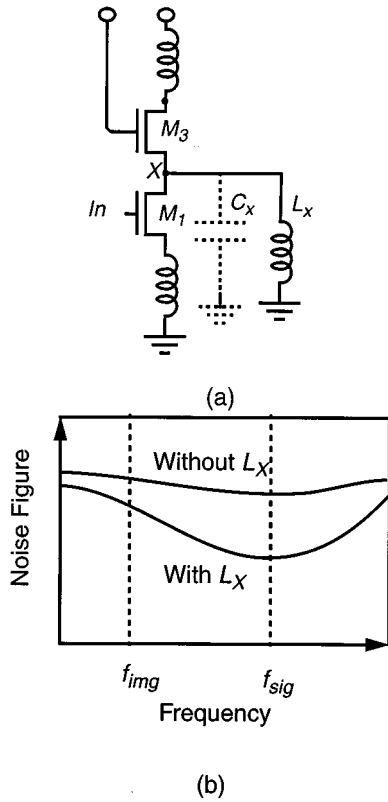


Fig. 5. (a) Improving the noise figure of a standard LNA and (b) noise figure versus frequency.

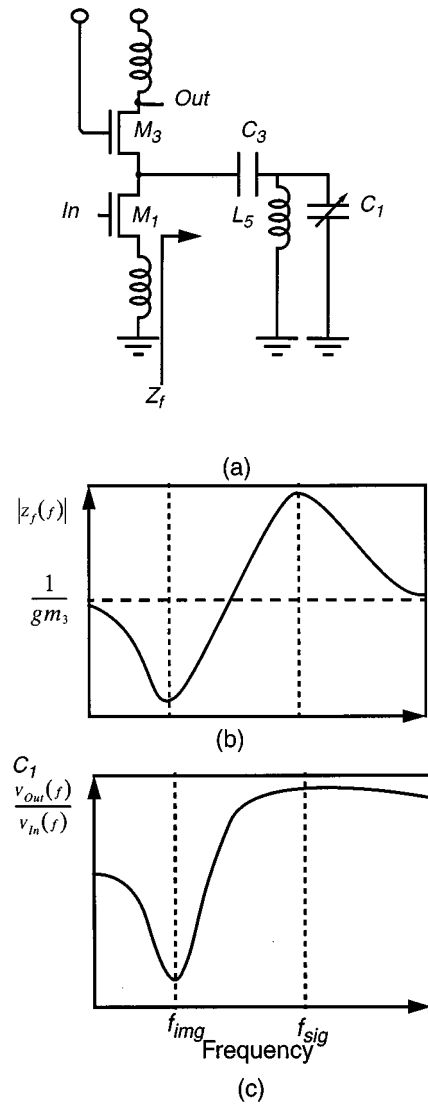


Fig. 6. (a) Circuit diagram of the LNA with a third-order filter, (b) input impedance of the filter versus frequency, and (c) the transfer function of the LNA/filter combination.

at node X and reduces the gain of the cascode structure. The presence of this parasitic capacitance makes the noise contribution of  $M_3$  more pronounced (see the Appendix.) To reduce the noise figure, the effect of this capacitance must be nullified. An inductor placed in parallel with this parasitic capacitance is a remedy to the problem. In Fig. 5(b), noise figure is plotted versus frequency. The noise performance of the LNA is improved with the help of the inductor.

Combining the ideas depicted in Figs. 4(a) and 5(a) would result in the circuit shown in Fig. 6(a). The filter comprises an inductor, a capacitor, and a varactor. The filter has a low impedance at the frequency of the image and a high impedance at the frequency of the signal. The input impedance of the filter  $Z_f$  can be written as

$$Z_f(s) = \frac{L_5 \cdot (C_3 + C_1)s^2 + 1}{C_1 \cdot C_3 \cdot L_5 \cdot s^3 + C_3 \cdot s} \quad (1)$$

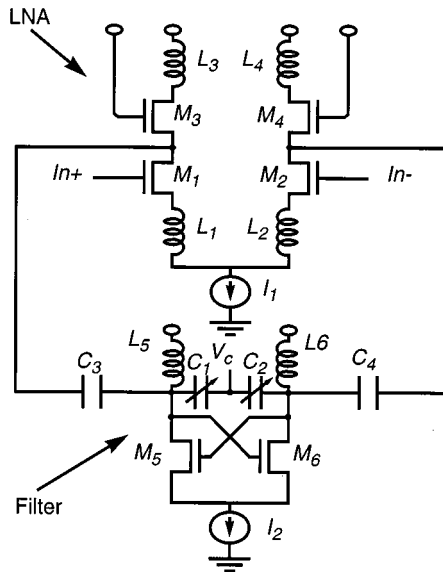


Fig. 7. Simplified circuit diagram of the LNA and filter.

The filter has imaginary zeros at

$$\omega_z = \pm \frac{1}{\sqrt{L_5 \cdot (C_3 + C_1)}} \quad (2)$$

and imaginary poles at

$$\omega_p = \pm \frac{1}{\sqrt{L_5 \cdot C_1}}. \quad (3)$$

The location of the pole-zero pair on the imaginary axes is controlled by the varactor.

Fig. 6(b) shows the input impedance of the filter  $|Z_f|$  as a function of the frequency. The resistance looking into the source of the cascode device,  $gm_3^{-1}$ , has also been marked on the same graph for comparison. For frequencies close to the location of the zero, the filter has an impedance lower than  $gm_3^{-1}$  and steals the ac current away from  $M_3$ , thus reducing the LNA gain. At frequencies close to the pole,  $|Z_f|$  is larger than  $gm_3^{-1}$  and the LNA gain is high. The resulting transfer function of the LNA/filter is shown in Fig. 6(c). The transfer function has a narrow valley, so for correct image cancellation, the zero must occur at the correct frequency. On the other hand, the peak is wide-band and the exact location of the pole is less important.

The third-order filter is designed not only to reject the image signal but also to diminish the effect of the parasitic capacitance at node X. Thus, by providing a pole (parallel resonance) as well as a zero (series resonance) the filter achieves image rejection and good noise performance at the same time. Although (1)–(3) need to be modified slightly to include the effect of this parasitic capacitance, the foregoing argument is still valid (see Appendix).

### III. CIRCUIT IMPLEMENTATION

#### A. LNA and Filter

Fig. 7 is a simplified schematic of the LNA and filter. A differential architecture is selected for better rejection of

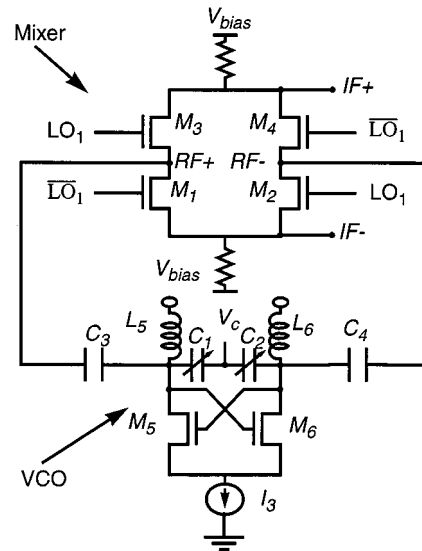


Fig. 8. A simplified circuit diagram of the VCO and PLL mixer.

on-chip interference. Also, the differential architecture alleviates the problem of parasitic source degeneration. To achieve the required high linearity, the LNA consists of only one stage, formed by transistors  $M_1$ – $M_4$ . Inductive degeneration is employed in the sources of  $M_1$  and  $M_2$  to produce a real term in the LNA's input impedance [11].

Capacitors  $C_1$ – $C_4$  and inductors  $L_5$  and  $L_6$  form a differential version of the filter discussed previously. The voltage  $V_c$  controls the location of the pole-zero pair by changing the capacitance of the accumulation mode varactors  $C_1$  and  $C_2$ .

The cross-connected differential pair,  $M_5$  and  $M_6$ , generates a negative impedance to cancel the losses in the filter, which are mainly due to the finite  $Q$  of the inductor. The depth of the notch in Fig. 6(c) depends on this negative impedance. By choosing a correct value for the tail current ( $I_2$  in Fig. 7), one can easily adjust the amount of image rejection without jeopardizing the stability of the filter. The LNA/filter combination becomes unstable when the net negative admittance of the filter (after subtracting the internal losses of the filter itself) becomes comparable to  $gm_3$ . Since the LNA core has a much higher bias current than the filter, there is a large margin of safety in this design. According to simulations, in our conservative design, the tail current can be increased by a factor of three before the LNA/filter combination becomes unstable.

The filter also reduces the noise figure of the cascode devices, at the cost of adding some extra noise of its own. However, the bias current of the  $M_5$  and  $M_6$  pair is much lower than that of the cascode devices,  $M_3$  and  $M_4$ , so the net effect is an improvement in the noise figure (see Appendix).

#### B. Image-Reject PLL

Fig. 8 is a simplified circuit diagram of the VCO and mixer used in the PLL loop. The same filter structure is now used as a VCO. The only difference is the increased tail current necessary to sustain oscillation. The mixer consists of four transistors,  $M_1$ – $M_4$ . The similarity between the topologies depicted in Figs. 7 and 8 suggests that the oscillation frequency of the VCO is a good measure of the zero location of the filter. A

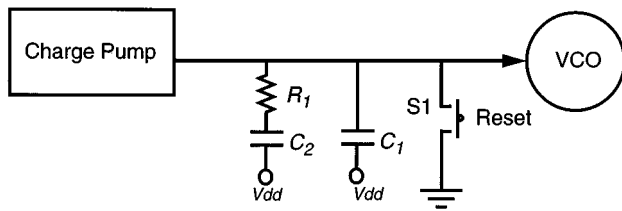


Fig. 9. Loop filter.

PFD, charge pump, and loop filter follow the mixer to complete the loop. Since these three blocks work at the frequency of the second LO, they consume little power (1.1 mW).

The offset PLL topology used for tuning can potentially lock to  $\omega_{LO1} + \omega_{LO2}$  instead of  $\omega_{LO1} - \omega_{LO2}$ . Several safety features are imbedded in the design of the PLL to avoid this threat. First, the VCO locking range is limited and  $\omega_{LO1} + \omega_{LO2}$  is outside the locking range of the VCO. In addition, as shown in Fig. 9, a switch is placed at the output of the loop filter to reset the VCO input to zero at the beginning of each channel select cycle. When the switch is released, the VCO input ramps up and the loop can only lock to  $\omega_{LO1} - \omega_{LO2}$ . Finally, to avoid overshoot on the control voltage that might otherwise force the PLL to lock to an incorrect frequency, the loop filter is designed such that the PLL is overdamped.

### C. Mixers

The output of the LNA is downconverted by the first set of mixers to produce the  $I$  and  $Q$  components of the IF signal. We chose a passive ring mixer topology for improved linearity. These signal-path mixers are identical to the mixer used in the PLL (Fig. 8). Each mixer consists of four transistors, grouped together into two pairs of transistors. During each half-cycle of the LO signal, the RF port is connected to the IF port with a different polarity, as described in detail in [11].

### D. Biasing Circuitry

The biasing of the receiver front end is accomplished on-chip through the use of a rather standard self-biased constant- $gm$  reference [12]. This type of reference generates the right current so that the transconductance  $gm$  is proportional to a reference conductance  $1/R$ . So, the output current of the bias circuit is whatever is necessary for the transconductance to follow  $1/R$ . Regulating  $gm$  reduces the dependence of the LNA gain, the transfer function of the filter, and input matching on supply and temperature variations.

### E. Input Matching Circuitry

The differential inputs of the LNA must be coupled to the single-ended output of the antenna. A single-ended to differential coupler (commonly known as a balun) is needed to achieve this task. A simple, yet effective way of designing a good balun at 5-GHz frequency range is to use off-chip microstrip lines. The ring hybrid structure depicted in Fig. 10(a) uses microstrip lines to generate two outputs that are  $180^\circ$  out of phase with respect to each other [13].

The ports A–B, B–C, and C–D are separated by  $90^\circ$ , and ports A and D are three-quarters of the wavelength away from

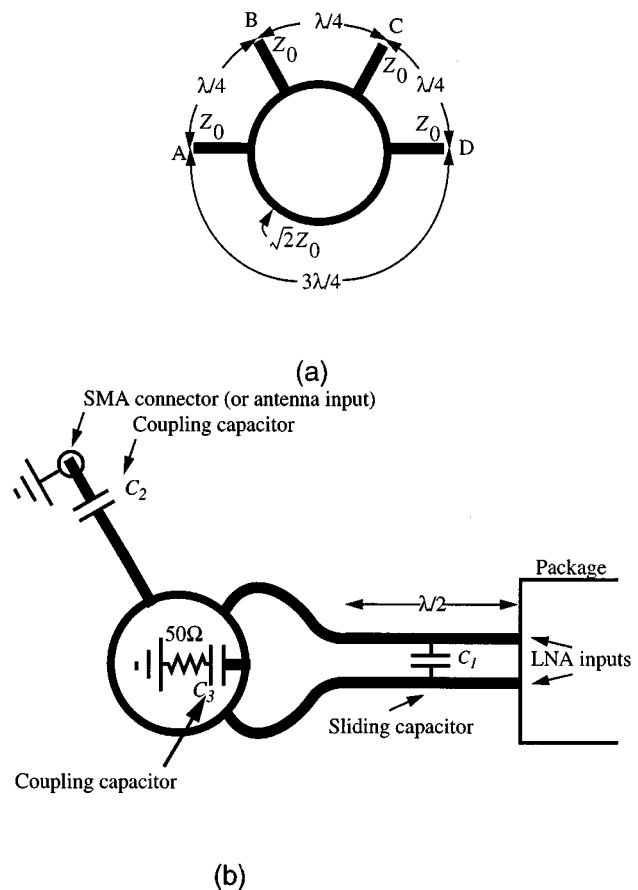


Fig. 10. (a) Ring-hybrid and (b) input matching circuitry.

each other. Because of the impedance and phase relationships shown in the structure, power fed to port A splits equally between ports B and D with a  $180^\circ$  phase difference, and port C remains isolated. Note that to maintain matching, the characteristic impedance of the ring is designed to be  $\sqrt{2}Z_0$ , where  $Z_0$  is the characteristic impedance of each port.

The off-chip matching circuitry is shown in Fig. 10(b). A sliding capacitor and two parallel transmission-line sections comprise a differential  $\pi$ -match. Matching can simply be done through trial and error. A  $50\text{-}\Omega$  resistor is used to terminate port C of the hybrid ring balun. The value of the sliding capacitor is determined based on the input impedance of the LNA and parasitic inductance and capacitance of the package and bond wires. In this design, the estimated pin inductance is 3 nH and bond-wire inductance is estimated to be 1 nH/mm.

## IV. MEASUREMENTS

The front-end receiver has been implemented in a  $0.24\text{-}\mu\text{m}$  CMOS technology; the die micrograph is shown in Fig. 11. The chip consumes 12.4 mW from a 2-V power supply and occupies  $1\text{ mm}^2$  of die area. It uses eight spiral inductors with patterned ground shields for improved quality factor and reduced crosstalk between spirals [14]. The  $Q$  of the inductors are estimated to be about five at the frequency of operation.

The LNA/filter combination has also been laid out as a separate test structure so that it could be characterized independently. As shown in Fig. 12, the differential LNA has a noise figure of

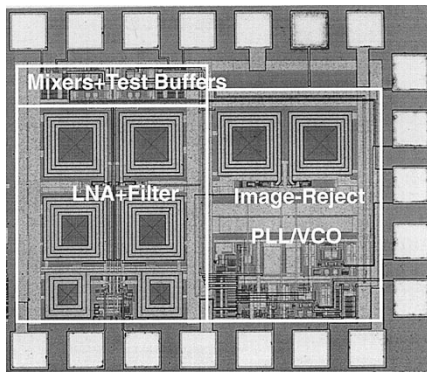


Fig. 11. Die micrograph of the receive path.

4.8 dB and consumes only 7.2 mW of power. For each point in this measurement, the image-reject PLL tunes the filter to the correct frequency.

For measurement purposes, test buffers placed after the two mixers allow characterization of the performance of the signal path. The overall measured noise figure is 5.2 dB. The input capacitance of each buffer is 0.3 pF. The amount of capacitive loading at the output of the mixers when implemented in a full system is lower than this value. Therefore, the test buffers provide more than a practical amount of loading, and the measurement results are realistic. For testing, the LO<sub>1</sub> signal is applied off chip. The amplitude of the LO<sub>1</sub> signal at the LO port of the mixer is 0.9 V-differential (450 mV single-ended). It is noteworthy to mention that passive ring mixers are highly linear but require relatively large LO amplitudes.

The filter consumes 1 mW of power, and the amount of image-rejection boost is 12 dB. The bandwidth of the image-reject notch is 200 MHz. As discussed before, in a more aggressive design, it is possible to increase the amount of rejection even further by increasing the power consumption of the filter. The image-reject PLL consumes 3.2 mW of power, of which 2.1 mW is burned by the VCO. The mismatch between the notch frequency of the filter and the VCO frequency is measured to be 0.9%, which is quite adequate for this application.

Fig. 13 shows the results of a two-tone third-order intercept point (IP3) measurement performed on the signal path. Two in-band signals are applied to the system at 5.250 and 5.255 GHz. The measured input-referred IP3 is  $-2$  dBm. The measured input-referred 1-dB compression point of the receiver is  $-14$  dBm (Fig. 14). The performance of the system is summarized in Table I.

The blocking performance of a receiver is determined by various factors, including its linearity, the phase noise of the VCO, and the spurious frequencies generated by the synthesizer. In this design, a synthesizer spur that falls in the adjacent channel band is the limiting blocking mechanism [8]. The spur is at  $-54$  dBc. An undesired adjacent channel that is 44 dB stronger than the desired signal is tolerated for a signal-to-interference ratio of 10 dB.

## V. CONCLUSIONS

A low-power and highly linear CMOS front-end receiver for a 5-GHz wireless LAN system has been presented. A third-order

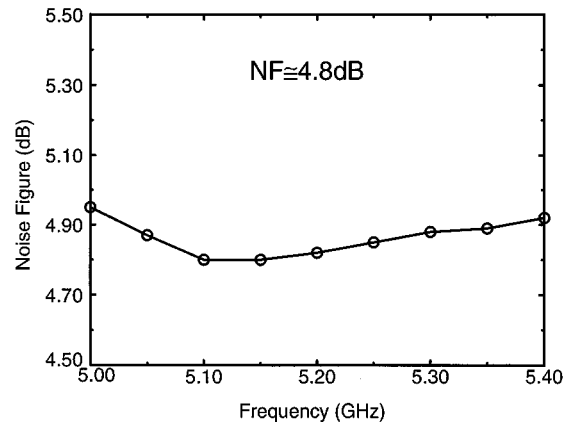


Fig. 12. Measured LNA noise figure.

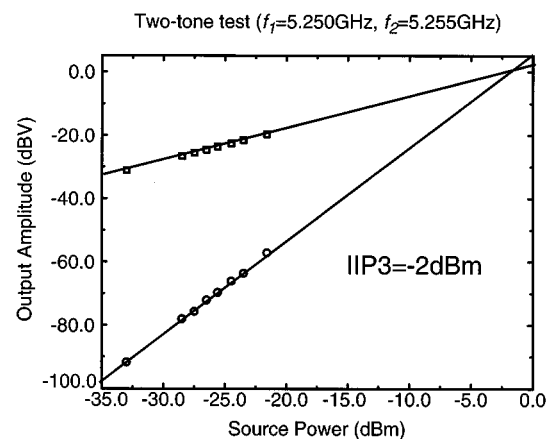


Fig. 13. Two-tone IP3 measurement for the RF front end.

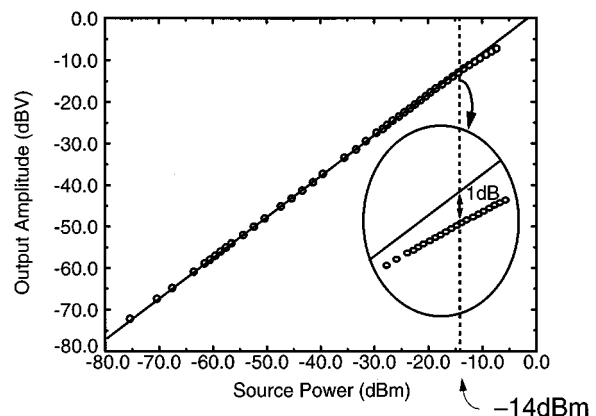


Fig. 14. One-dB compression-point measurement.

filter alters the transfer function of the LNA to reject the image signal and to decrease the noise contribution of the cascode devices in the LNA core. A PLL structure automatically tunes the filter to the correct frequency.

## APPENDIX NOISE CONSIDERATIONS

A simple noise analysis of the circuit shown in Fig. 15(a) quantifies the effects of parasitic capacitance  $C_x$ . An equivalent circuit for noise calculation at the resonance frequency  $\omega_0$ , is

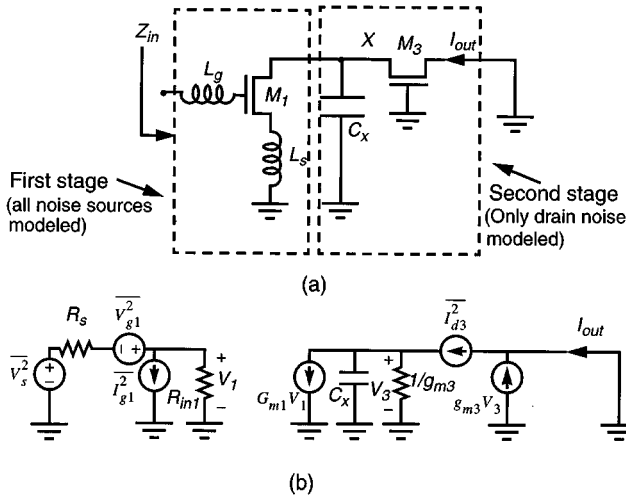


Fig. 15. (a) Standard LNA topology and (b) equivalent circuit for noise calculations.

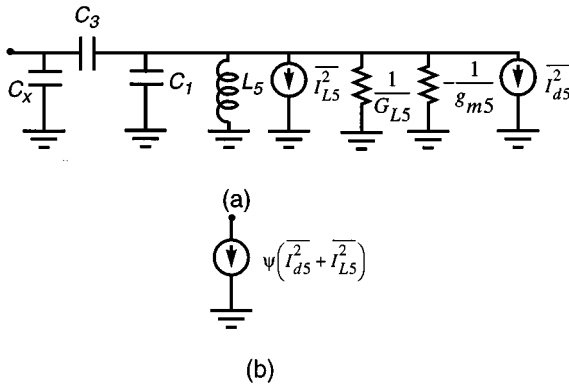


Fig. 16. (a) Filter noise model and (b) simplified filter noise model at the frequency of the pole.

depicted in Fig. 15(b). All parasitic capacitances of node X, as well as junction capacitors and the gate–source capacitance of  $M_3$ , are absorbed into  $C_x$ .

At the resonant frequency of the input circuit, the impedance is purely real and is calculated to be

$$R_{in1} = \frac{gm_1}{C_{gs1}} \cdot L_s. \quad (4)$$

In Fig. 15(b), all the noise sources of the first stage are modeled through equivalent input-referred voltage and current noise sources, but only the drain noise of the second stage is modeled. Including all other noise sources of the second stage only complicates the derivations while adding little accuracy to the derived formulas. The equivalent transconductance of the first stage when the input is matched is

$$G_m \approx \frac{\omega_T}{\omega_0 R_s} \quad (5)$$

where  $\omega_T = g_{m1}/C_{gs1}$ ,  $\omega_0$  is the input resonant frequency and  $R_s$  is the source impedance.

The drain noise current of the second stage is

$$\frac{\overline{I_{d3}^2}}{\Delta f} = 4kT\gamma_3 g_{d\phi 3} \quad (6)$$

where  $g_{d\phi 3}$  is the zero-bias drain conductance of the device and  $\gamma_3$  is a bias-dependent factor. The noise factor of the first stage  $F_1$  is

$$F_1 = 1 + \frac{1}{4kTR_s} \overline{V_{g1}^2} + \frac{R_s^2}{4kTR_s} \overline{I_{g1}^2}. \quad (7)$$

Calculating the total noise figure of the circuit and simplifying the result using (7), one obtains

$$F_{no-filter} = F_1 + 4R_s \gamma_3 g_{d\phi 3} \left( \frac{\omega_0^2}{\omega_T^2} \right) \left( \frac{C_x^2}{g_{m3}^2} \omega_0^2 \right). \quad (8)$$

Equation (8) shows that capacitance  $C_x$  has a big impact on the noise figure at high frequencies. The effect of this capacitance can be nullified by an inductor. With the help of a parallel inductor that resonates with  $C_x$  at the frequency of interest, the noise factor reduces to that of the first stage. That is, the noise contribution of  $M_3$  is negligible when  $C_x$  is effectively removed.

To derive the noise contribution of the filter, (1)–(3) must be modified to include the effect of  $C_x$ . A more accurate expression for the input impedance of the filter  $Z_f$  can be written as

$$Z_f(s) = \frac{L_5 \cdot (C_3 + C_1) \cdot s^2 + 1}{(C_1 C_3 + C_1 C_x + C_3 C_x) \cdot L_5 \cdot s^3 + (C_3 + C_x) \cdot s} \quad (9)$$

whose imaginary poles are located at

$$\omega_p = \pm \frac{1}{\sqrt{L_5 \left( C_1 + \frac{C_3 C_x}{C_3 + C_x} \right)}}. \quad (10)$$

Fig. 16(a) shows a simplified model for the filter noise. Drain noise of  $M_5$  (Fig. 6) has a form similar to (6) and is expressed as

$$\frac{\overline{I_{d5}^2}}{\Delta f} = 4kT\gamma_5 g_{d\phi 5}. \quad (11)$$

The noise contribution of the inductor is

$$\frac{\overline{I_{L5}^2}}{\Delta f} = 4kTG_{L5} \quad (12)$$

where  $G_{L5} = Q_{L5} L_5 \omega_0$ . Since the  $Q$  of the varactor is assumed to be larger than the finite  $Q$  of the inductor [16], inductor noise is dominant.

Assuming that the filter is tuned correctly,  $\omega_0 = \omega_p$ , and using (10), the noise model (Norton equivalent) of the filter is simplified as shown in Fig. 16(b), where

$$\psi = \frac{C_3^2 \cdot \omega_0^2}{\left( \frac{C_3^2}{C_x + C_3} \right)^2 \cdot \omega_0^2 + (G_{L5} - g_{m5})^2}. \quad (13)$$

Note that the impedance of the filter at the frequency of the pole is high enough [compared to  $gm_3^{-1}$  in Fig. 15(b)] and the equivalent Norton impedance is ignored. The overall noise figure of the LNA/filter combination is

$$F_{tot} = F_1 + \psi \cdot 4R_s (\gamma_5 g_{d\phi 5} + G_{L5}) \left( \frac{\omega_0^2}{\omega_T^2} \right). \quad (14)$$

The measured noise figure of the LNA with the filter is 4.8 dB, whereas the measured noise figure of the LNA without the filter is 5.5 dB. The filter therefore not only performs image rejection but also improves the noise figure by 0.7 dB. To obtain an expression for  $F_1$ , please refer to [15].

#### ACKNOWLEDGMENT

The authors would like to thank S. S. Mohan and M. Hershenson for their help on the design of inductors and D. K. Shaeffer, D. M. Colleran, and A. R. Shahani for helpful discussions. They are also thankful to National Semiconductor for fabricating the chip.

#### REFERENCES

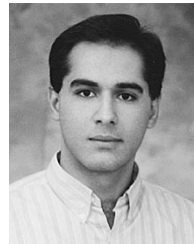
- [1] K. Pahlavan, A. Zahedi, and P. Krishnamurthy, "Wideband local access: Wireless LAN and wireless ATM," *IEEE Commun. Mag.*, pp. 34–40, Nov. 1997.
- [2] B. Razavi, "Design consideration for direct-conversion receivers," *IEEE Trans. Circuits Syst.*, vol. 44, pp. 428–435, June 1997.
- [3] M. McDonald, "A 2.5GHz BiCMOS image-reject front end," in *ISSCC Dig. Tech. Papers*, Feb. 1993, pp. 144–145.
- [4] V. Aparin and P. Katzin, "Active GaAs MMIC band-pass filters with automatic frequency tuning and insertion loss control," *IEEE J. Solid-State Circuits*, vol. 30, pp. 1068–1073, Oct. 1995.
- [5] C. Chiou and R. Schaumann, "Design performance of a fully integrated bipolar 10.7 MHz analog band-pass filter," *IEEE J. Solid-State Circuits*, vol. SC-21, pp. 6–14, Oct. 1986.
- [6] Y. Wang and A. Abidi, "CMOS active filter design at very high frequencies," *IEEE J. Solid-State Circuits*, vol. 25, pp. 1562–1574, Dec. 1990.
- [7] S. Jones, "RF system requirements for HIPERLAN," in *Microwave and RF Conf. Proc.*, 1995, pp. 1–6.
- [8] H. Rategh, H. Samavati, and T. Lee, "A CMOS frequency synthesizer with an injection-locked frequency divider for a 5 GHz Wire LAN receiver," *IEEE J. Solid-State Circuits*, vol. 35, pp. 779–786, May 2000.
- [9] H. Rategh and T. Lee, "Superharmonic injection locked frequency dividers," *IEEE J. Solid-State Circuits*, vol. 34, pp. 813–821, June 1998.
- [10] J. Macedo and M. Copeland, "A 1.9-GHz silicon receiver with monolithic image filtering," *IEEE J. Solid-State Circuits*, vol. 33, pp. 378–386, Mar. 1998.
- [11] A. Shahani, D. Shaeffer, and T. Lee, "A 12-mW wide dynamic range front-end for a portable GPS receiver," *IEEE J. Solid-State Circuits*, vol. 32, pp. 2061–2070, Dec. 1997.
- [12] D. Shaeffer, A. Shahani, S. Mohan, H. Samavati, H. Rategh, M. Hershenson, M. Xu, C. Yue, D. Eddleman, and T. Lee, "A 115-mW, 0.5-mm CMOS GPS receiver," *IEEE J. Solid-State Circuits*, vol. 33, pp. 2219–2231, Dec. 1998.
- [13] I. Bahl and P. Bhartia, *Microwave Solid State Circuit Design*. New York, NY: Wiley, 1988, pp. 178–185.
- [14] C. Yue and S. Wong, "On-chip spiral inductors with patterned ground shields for Si-based RF IC's," in *Symp. VLSI Circuits Dig.*, June 1997, pp. 85–86.
- [15] D. Shaeffer and T. Lee, "A 1.5V, 1.5 GHz CMOS low noise amplifier," *IEEE J. Solid-State Circuits*, vol. 32, pp. 745–759, May 1997.
- [16] T. Soorapanth and T. Lee, "RF linearity of short-channel MOSFET's," in *Int. Workshop Design of Mixed-Mode Integrated Circuits and Applications Dig. Tech. Papers*, July 1997, pp. 81–84.



**Hiran Samavati** (S'99) received the B.S. degree in electrical engineering from Sharif University of Technology, Tehran, Iran, in 1994 and the M.S. degree in electrical engineering from Stanford University, Stanford, CA, in 1996, where he is currently working toward the Ph.D. degree.

During the summer of 1996, he was with Maxim Integrated Products, where he designed building blocks for a low-power infrared transceiver IC. His research interests include RF circuits and analog and mixed-signal VLSI, particularly integrated transceivers for wireless communications.

Mr. Samavati received a departmental fellowship from Stanford University in 1995 and a fellowship from IBM Corporation in 1998. He received the ISSCC Jack Kilby outstanding student paper award for the paper "Fractal Capacitors" in 1998.



**Hamid R. Rategh** (S'99) was born in Shiraz, Iran, in 1972. He received the B.S. degree in electrical engineering from Sharif University of Technology, Iran, in 1994 and the M.S. degree in biomedical engineering from Case Western Reserve University, Cleveland, OH, in 1996. He is currently pursuing the Ph.D. degree in the Department of Electrical Engineering, Stanford University, Stanford, CA.

During the summer of 1997, he was with Rockwell Semiconductor System in Newport Beach, CA, where he was involved in the design of a CMOS dual-band, GSM/DCS1800, direct conversion receiver. His current research interests are in low-power radio-frequency integrated circuits design for high-data-rate wireless LAN systems. He was a member of the Iranian team in the 21st International Physics Olympiad, Groningen, the Netherlands.

Mr. Rategh received the Stanford Graduate Fellowship in 1997.



**Thomas H. Lee** (M'96) received the S.B., S.M., and Sc.D. degrees in electrical engineering from the Massachusetts Institute of Technology in 1983, 1985, and 1990, respectively.

He joined Analog Devices in 1990, where he was primarily engaged in the design of high-speed clock recovery devices. In 1992, he joined Rambus Inc., Mountain View, CA, where he developed high-speed analog circuitry for 500-Mb/s CMOS DRAM's. He has also contributed to the development of PLL's in the StrongARM, Alpha, and K6/K7 microprocessors.

Since 1994, he has been an Assistant Professor of Electrical Engineering at Stanford University, where his research focus has been on gigahertz-speed wireline and wireless integrated circuits built in conventional silicon technologies, particularly CMOS. He has received 12 U.S. patents and is the author of *The Design of CMOS Radio-Frequency Integrated Circuits* (Cambridge, U.K.: Cambridge Univ. Press, 1998), and is a coauthor of two additional books on RF circuit design. He is also a cofounder of Matrix Semiconductor.

He has twice received the "Best Paper" award at the International Solid-State Circuits Conference (ISSCC), was co-author of a "Best Student Paper" at ISSCC, and recently won a Packard Foundation Fellowship. He is a distinguished lecturer of the IEEE Solid-State Circuits Society, and was recently named a Distinguished Microwave Lecturer.